

All-Optical Linear-Polarization Engineering in Single and Coupled Exciton-Polariton Condensates

I. Gnusov^{1,*}, H. Sigurdsson^{2,3,†}, J.D. Töpfer¹, S. Baryshev¹, S. Alyatkin¹, and P.G. Lagoudakis^{1,3}

¹Skolkovo Institute of Science and Technology, Moscow, Territory of innovation center “Skolkovo”, Bolshoy Boulevard 30, bld. 1, 121205, Russia

²Science Institute, University of Iceland, Dunhagi 3, Reykjavik IS-107, Iceland

³School of Physics and Astronomy, University of Southampton, Southampton SO17 1BJ, United Kingdom



(Received 20 January 2021; revised 5 August 2021; accepted 12 August 2021; published 8 September 2021)

We demonstrate all-optical linear-polarization control in semiconductor microcavities using an exciton-polariton condensate in an elliptically shaped optical trap. The microcavity inherent TE-TM splitting lifts the pseudospin degeneracy of the anisotropic trap ground state. The emerging fine-structure modes are shown to be polarized linearly parallel and perpendicular to the trap major axis. We demonstrate polariton condensation into the excited pseudospin mode with a high degree of linear polarization, which rotates as we rotate the trap. We then extend our study to a system of two coupled linearly polarized condensates and demonstrate rich spin dynamics reflecting spontaneous synchronization and high correlation between the condensate pseudospins as a function of the pump parameters. Our findings open up exciting perspectives in both spintronics and studies on extended systems of interacting nonlinear optical elements with anisotropic coupling strength and adjustable fine structure.

DOI: 10.1103/PhysRevApplied.16.034014

I. INTRODUCTION

Exciton-polaritons (polaritons hereafter), often referred to as liquid light, are a mixture of both light and matter. They arise in the strong-coupling regime between quantum-well excitons and cavity photons in semiconductor microcavities [1]. Being composite bosons, they can undergo a power-driven nonequilibrium phase transition into a highly coherent many-body state referred to as a polariton condensate [2]. An essential characteristic of these liquid-light particles is their pseudospin (or just spin) projection ($\pm\hbar$) onto the growth axis of the cavity, which can easily be determined by measuring the polarization of the polariton photoluminescence (PL).

The strong nonlinear nature of polaritons through their spin-anisotropic excitonic Coulomb interactions results in numerous intriguing spinor condensate properties that will be desirable in future spinoptronic technologies [3,4]. This includes spin bistability [5–7] and multistability [8], switches [9,10], the optical spin Hall effect [11], polarized solitons [12,13] and vortices [14–16], spin bifurcation points [17], and topological phases [18,19]. Different parts for polariton-based spin circuitry have already been realized [9,10,20–22], with some exciting recent

theoretical proposals [23,24], but many challenges remain to be solved. Optical applications such as data communication or sensing benefit from precise control over the polarization and modulation speeds of a laser, ideally using nonresonant-excitation schemes such as spin vertical-cavity surface-emitting lasers (VCSELs) [25–27]. In this spirit, a great deal of effort has been devoted to generating sources of linearly polarized light such as colloidal nanorods [28], materials with anisotropic optical properties [29], quantum dots [30], and optical parametric oscillators [31].

Under nonresonant excitation in inorganic semiconductors, spin transfer from the pumping laser to the condensate is possible by using an elliptically polarized beam that creates a spin-imbalanced polariton gain (i.e., optical orientation of excitons) [6,32]. This allows the generation of condensates with a high degree of circular polarization, aligned with the pump. However, the linearly polarized polariton modes experience isotropic gain, making them insensitive to the linear-polarization details of the nonresonant-excitation source [33,34] except in the presence of cavity strain and birefringence [32,35–39] or engineered anisotropic cavities [40,41]. The same also applies for VCSELs, where the linear polarization of the emission is engineered by etching asymmetric masks [42,43] or electrodes [44], heating [45], or applying mechanical stress [26]. Alternatively, in organic polaritonics,

*Ivan.Gnusov@skoltech.ru

†h.sigurdsson@soton.ac.uk

single-molecule Frenkel excitons can be excited by a linearly polarized nonresonant pump coaligned with their dipole moment, leading to polariton condensation of the same linear polarization [46]. However, control over both the circular- and linear-polarization degrees of freedom in a polariton condensate through nonresonant all-optical means has remained elusive.

Here, we demonstrate *in situ* optical control of the linear polarization in inorganic polariton condensates in a cavity with polarization-dependent reflectivity, or TE-TM splitting [11,47]. By spatially shaping the nonresonant-excitation laser profile into the form of an ellipse, we are able to fully control the direction of the condensate linear polarization. Our elliptically shaped pump induces an anisotropic in-plane trapping potential and gain media for the polaritons. Such an excitation profile along with the cavity TE-TM splitting leads to condensation (lasing) into a mode of definite linear polarization parallel to the minor axis of the trap ellipse. The optical malleability of the trap geometry allows for noninvasive deterministic control over the linear polarization of the condensate by just utilizing the nonresonant-excitation laser. Moreover, we investigate the effects of anisotropic coupling between two spatially separated condensates and identify several different regimes of exotic linear-polarization dynamics.

II. EXPERIMENT

Our experiments are conducted on an inorganic $2\lambda\text{GaAs}/\text{AlAs}_{0.98}\text{P}_{0.02}$ microcavity with embedded InGaAs quantum wells [48]. The sample is excited nonresonantly by a linearly polarized continuous-wave (cw) laser ($\lambda = 783.6$ nm). The optical-excitation beam is chopped using an acousto-optic modulator to form 10- μs square pulses at a 1-kHz repetition rate to diminish heating of the sample held at a temperature of 4 K. The exciton-cavity mode detuning is -3 meV. A reflective liquid-crystal spatial light modulator (SLM), commonly used today for optical shaping of polariton condensates, transforms the transverse profile of the pump laser beam to have an elliptically shaped confinement region [see Fig. 1(a)] and dashed ellipse in Fig. 1(b)]. We investigate the sample PL in real [Figs. 1(c) and 1(d)] and reciprocal [Fig. 1(e)] space and record the time- and space-averaged polarization of the PL by simultaneously detecting all the polarization components [32].

The polariton-condensate order parameter is written in the canonical spin-up and spin-down basis $\Psi = (\psi_+, \psi_-)^T$, corresponding to left- and right-circularly polarized condensate emission, respectively. It is convenient to use the pseudospin formalism corresponding to the Stokes vector of the emitted light $\mathbf{S} = (S_1, S_2, S_3)^T = \langle \Psi^\dagger \hat{\sigma} \Psi \rangle / \langle \Psi^\dagger \Psi \rangle$, where $\hat{\sigma}$ is the Pauli matrix vector. The polariton PL is analyzed in terms of time-averaged Stokes

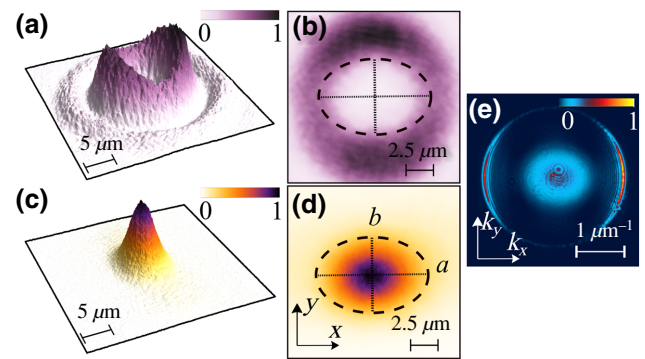


FIG. 1. The spatial intensity profiles of the (a),(b) excitation laser and (c),(d) condensate PL. The excitation laser induces a trapping potential with horizontal and vertical radii denoted a,b respectively. (e) The momentum distribution of the condensate PL. Panels (c)–(e) correspond to a condensate pumped twice above its condensation threshold (i.e., $P = 2P_{\text{th}}$).

components, which are written as

$$S_1 = \frac{I_H - I_V}{I_H + I_V}, \quad S_2 = \frac{I_D - I_A}{I_D + I_A}, \quad S_3 = \frac{I_{\sigma+} - I_{\sigma-}}{I_{\sigma+} + I_{\sigma-}}, \quad (1)$$

where $I_{H,V,D,A,\sigma^+,\sigma^-}$ are the time-averaged intensities of horizontal, vertical, diagonal, antidiagonal, and right- and left-circular-polarization projections of the emitted light, respectively.

We start by exciting the sample with a symmetric ring-shaped pump profile [see the inset in Fig. 2(a)], creating a two-dimensional trap for the polaritons. Ramping the pump power above the condensation threshold denoted as P_{th} , we obtain condensation into the fundamental trap mode. The optical trap is realized by the strong polariton repulsive interactions with the background pump-induced cloud of incoherent excitons. This reservoir of excitons forms a blue-shifting potential onto the polaritons [49,50], while at the same time providing gain. Such an optical trapping technique has the advantage of reducing the overlap between the condensate and the exciton reservoir, minimizing detrimental dephasing effects [51]. By scanning the excitation position with the ring-shaped pump profile, we locate a spot on our sample with a small degree of polarization $DOP = \sqrt{S_1^2 + S_2^2 + S_3^2}$ [see Fig. 2(a)] of the emitted light. The small $S_{1,2}$ above threshold implies that the trap ground state is spin degenerate, such that from realization to realization, random linear polarization builds up, which averages out over many shots. A small S_3 confirms that our laser is (to a good degree) linearly polarized and does not break the spin-parity symmetry of the system. The effects of using elliptically polarized pumps are discussed in Sec. S1 in the Supplemental Material [52]. We also note that in our presented data, we compensate for the effects of optical retardance arising in our setup (for further details, see Sec. S2 in the Supplemental Material [52]).

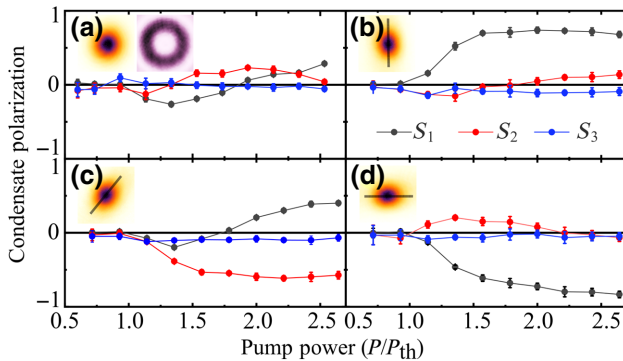


FIG. 2. (a) The power dependence of the condensate $S_{1,2,3}$ Stokes parameters (black, red, and blue markers) for the annular pump with a resultant cylindrically symmetric condensate profile (see the right and left insets, respectively). (b)–(d) The same, but now for a trap or condensate with a major axis orientated at (b) 90° , (c) 45° , and (d) 0° . The insets in (b)–(d) depict the real-space condensate PL, with black lines showing the orientation of the trap major axis.

III. CONDENSATE LINEAR-POLARIZATION CONTROL

A. Rotation of the elliptical trap

We then transform the excitation profile to the one shown in Figs. 1(a) and 1(b). Nonuniform distribution of the intensity in the excitation leads to the formation of an elliptically shaped optical trap denoted by the dashed ellipse, squeezing the condensate as shown in Fig. 1(d). We now observe a massive increase of the linear-polarization components of the condensate above $1.2P_{\text{th}}$ at the same sample position. The direction of the linear polarization of the emission is found to follow the trap minor axis. Namely, for the vertically elongated condensate in Fig. 2(b), we observe an increase of the S_1 Stokes component (horizontal polarization). The same effect is present for the diagonally and horizontally elongated condensates in Figs. 2(c) and 2(d). We note that the results are independent of the angle of linear polarization of the pump laser (see Sec. S1 in the Supplemental Material [52]).

By rotating the excitation profile with the SLM, we can engineer any desired linear polarization in the condensate. In Fig. 3(a), we present the measured polarization components of the condensate as a function of the condensate major-axis angle. We observe a continuous rotation of the condensate polarization close to the equatorial plane of the Poincaré sphere, following the minor axis of the trap. We point out that $\text{DOP} < 1$ appears from various depolarizing effects, such as noise due to scattering from the incoherent reservoir to the condensate [39], polariton-polariton interactions in the condensate causing self-induced Larmor precessions [57], and mode competition [58].

We also check that the results of our study are not dependent on the precise shape of our optical trap. In Sec. S3

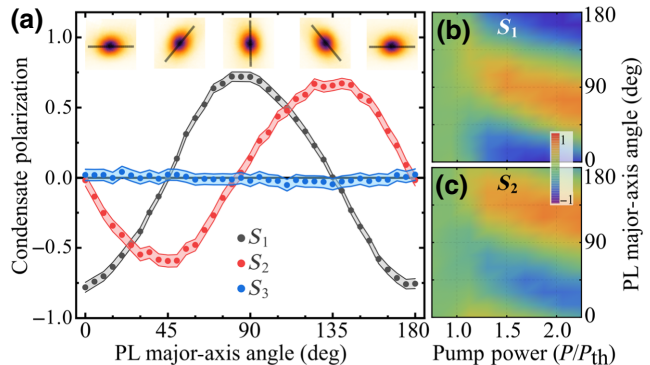


FIG. 3. (a) Condensate Stokes parameters for different orientations of the condensate major axis in real space (insets) at $P = 1.94P_{\text{th}}$. The black lines depict the major axis of the trap. The colored regions show the error of the measurement. (b) S_1 and (c) S_2 color maps for varying pump power and major-axis orientation, showing counterclockwise rotation of the pseudospin with increasing power.

in the Supplemental Material [52], we test another geometrical construction of the excitation profile in the form of eight Gaussian beams arranged to form an ellipse and retrieve qualitatively the same result as presented here in the main text.

Figures 3(b) and 3(c) show the pump-power and trap-orientation dependence of the $S_{1,2}$ Stokes parameters. Interestingly, with increasing pump power, we observe counterclockwise rotation of the pseudospin in the equatorial plane of the Poincaré sphere. The rotation is approximately 30° between 1.2 and $2.2P_{\text{th}}$. This effect appears due to a small amount of circular polarization in our pump, which creates a spin-imbalanced trapping potential, and gain media, which act as a complex population-dependent out-of-plane magnetic field Ω_\perp that applies torque on the condensate pseudospin. This is confirmed through simulations using the generalized Gross-Pitaevskii equation (see Sec. S10 in the Supplemental Material [52]). Further analysis of this power-dependent trend of the $S_{1,2}$ is beyond the scope of the current study.

B. Theory of a single condensate in an elliptically shaped optical trap

Our observations can be interpreted in terms of photonic TE-TM splitting acting on the optically confined polaritons, which, when the trap $V(\mathbf{r})$ has broken cylindrical symmetry, leads to fine-structure splitting in the trap transverse modes. This determines a state of definite polarization into which the polaritons condense. In the noninteracting regime, polaritons obey the following Hamiltonian:

$$\hat{H} = \frac{-\hbar^2 \nabla^2}{2m} - \hat{\sigma} \cdot \Omega + V(\mathbf{r}) - \frac{i\hbar\Gamma}{2}, \quad (2)$$

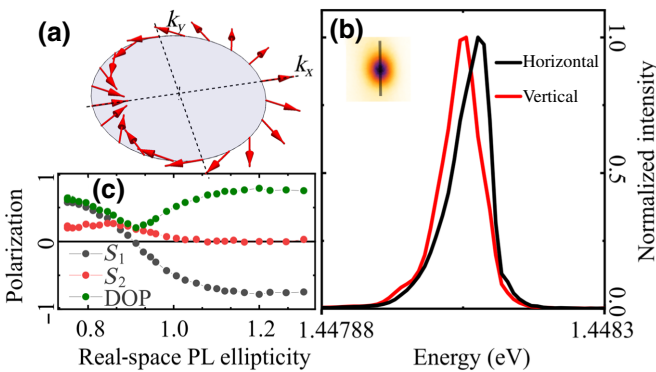


FIG. 4. (a) The distribution of the in-plane effective magnetic field $\Omega(\mathbf{k})$ (red arrows) in momentum space due to TE-TM splitting given by Eq. (3). (b) The horizontal (black) and vertical (red) polarization resolved normalized spectra of the condensate emission at $k = 0$ for a vertically elongated trap ($\theta_{\min} = 0$). The splitting between levels is approximately $20 \mu\text{eV}$. (c) The linear-polarization components and the DOP for different real-space ellipticities of the condensate. The data are taken at $P \approx 1.8P_{\text{th}}$.

where m is the effective mass, $\mathbf{k} = (k_x, k_y)$ is the in-plane cavity momentum, Γ^{-1} is the polariton lifetime, and

$$\Omega(\mathbf{k}) = \hbar^2 \Delta \begin{pmatrix} k_x^2 - k_y^2 \\ 2k_x k_y \\ 0 \end{pmatrix} \quad (3)$$

is the effective magnetic field in momentum space [see Fig. 4(a)] from the TE-TM splitting of strength Δ [11] acting on the polariton pseudospin. Note that the minus sign in front of the magnetic potential energy is conventional but many other works use a positive sign with no loss of generality. For elliptical confinement, which we assume to be harmonic for simplicity, $V(\mathbf{r}) = m(\omega_x^2 x^2 + \omega_y^2 y^2)/2$, the TE-TM splitting lifts the degeneracy of the trap spin levels. For the lowest trap state, the magnetic field reads (for a detailed derivation, see Sec. S5 in the Supplemental Material [52])

$$\Omega_{\text{trap}} \simeq -\frac{\hbar m |\Delta| \delta\omega}{2} \begin{pmatrix} \cos(2\theta_{\min}) \\ \sin(2\theta_{\min}) \\ 0 \end{pmatrix}. \quad (4)$$

Here, θ_{\min} is the angle of the trap minor axis from the horizontal and $\delta\omega = |\omega_x - \omega_y| \propto |a^{-1} - b^{-1}|$ is the absolute difference between the trap oscillator frequencies along the major and the minor axes [Fig. 1(d)]. We point out that the minus sign in Eq. (4) is written explicitly because $\Delta < 0$ in our sample [59] (see Sec. S4 in the Supplemental Material [52]).

The direction of the effective magnetic field is controlled by the angle of our elliptical trap, θ_{\min} , which consequently rotates the condensate pseudospin in the equatorial plane

of the Poincaré sphere such that it stabilizes antiparallel to the magnetic field $-\mathbf{S} \parallel \Omega_{\text{trap}}$. This leads to smooth changes in the $S_{1,2}$ Stokes components of the emitted light as the trap rotates as shown in Fig. 3. The results of our experiment are accurately reproduced through a mean-field theory using a generalized Gross-Pitaevskii model describing the polariton-condensate spinor order parameter Ψ coupled with a background excitonic reservoir (see Sec. S6 in the Supplemental Material [52]).

Interestingly, in a recent experiment [32], we have observed condensation into the spin ground state of a circular trap, where the fine-structure splitting originated from the cavity birefringence $\Omega_{\text{bir}}(\mathbf{r})$. This meant that the condensate pseudospin stabilized parallel to the magnetic field $\mathbf{S} \parallel \Omega_{\text{bir}}(\mathbf{r})$. In the current experiment, however, we instead observe condensation into the excited spin state, i.e., antiparallel to the magnetic field $-\mathbf{S} \parallel \Omega_{\text{trap}}$. This can be directly evidenced in Fig. 4(b), where we show the normalized polarization-resolved spectrum of a vertically elongated trap that obtains a horizontally polarized condensate that is higher in energy.

By performing linear stability analysis on a Gross-Pitaevskii mean-field model (see Sec. S7 in the Supplemental Material [52]), we determine that repulsive polariton-polariton interactions normally lead to condensation in the fine-structure ground state [39]. However, the additional presence of an uncondensed background of reservoir excitons contributes to an effective attractive mean-field interaction in the condensate [60], which causes the ground state to become unstable, favoring condensation into the excited state, as we observe in the current experiment. Another effect is the different penetration depths of the linearly polarized polariton modes (due to their different effective masses from the TE-TM splitting) into the excess gain region about the trap short axis. This leads to higher gain for the fine-structure excited state, which facilitates its condensation. Several parameters of the polariton system, such as the exciton-photon detuning, the quantum-well material, and the shape of the pump profile, allow tuning from one stability regime to another, which explains why some experiments show ground-state condensation [32] while others, like ours, show excited-state condensation [61]. We stress that regardless of whether the system parameters favor condensation into the spin ground or excited state of the optical trap, the main result of our study remains valid.

C. Changing the trap spatial ellipticity

So far, we have shown control over the linear polarization of the condensate by rotating the trap major axis and varying the pump power. Here, we show that the condensate linear polarization can also be controlled by tuning the trap spatial ellipticity (i.e., the ratio of the major and minor axes). In Fig. 4(c), we continuously change the trap

spatial ellipticity from a vertically elongated trap ($a < b$) to a horizontally elongated one ($a > b$). The PL spatial-ellipticity axis denotes the ratio of the widths of the PL along the x and y axes [see Fig. 1(d)]. The pseudospin of the condensate steadily changes from horizontal to vertical polarization, going through a low-DOP regime. We stress that the data in Fig. 4(c) are obtained at a different position of the cavity sample compared to Figs. 1–3, which leads to finite S_1 at zero PL ellipticity ($a = b$) even though $\Omega_{\text{trap}} = 0$. This is because of local birefringence in the cavity mirrors, giving rise to an additional static in-plane magnetic field $\Omega_{\text{bir}}(\mathbf{r})$. Therefore, one needs to account for a net field $\Omega_{\text{net}} = \Omega_{\text{bir}}(\mathbf{r}) + \Omega_{\text{trap}}$ orientating the condensate pseudospin. The point of low DOP in Fig. 4(c) corresponds, then, to near cancellation between the local birefringence and the TE-TM splitting $\Omega_{\text{net}} \approx 0$.

IV. COUPLED CONDENSATES

A. Experimental observations

Networks of coupled polariton condensates [50,62] can be seen as an attractive platform to study synchronization phenomena between nonlinear optical elements such as microlaser arrays [63] and to investigate the behavior of complex nonequilibrium many-body polariton systems and excitations in non-Hermitian lattices [24,64–66]. Inspired by these studies, we create two identical, spatially separated, elliptical optical traps utilizing two SLMs, resulting in the formation of two coupled condensates [Fig. 5].

There are two intriguing possibilities in our interacting system. First, we can adjust the fine structure of each optical trap through its major-axis angle. Second, the interaction strength between different condensates depends on their relative major-axis angle, since the trap anisotropy allows polaritons to escape faster along its major axis [see Fig. 1(b)]. This can also be evidenced in Fig. 1(e) as a high concentration of coaligned PL in momentum space. This leads to stronger coupling when the trap major axes are orientated longitudinally to the coupling direction and weaker when orientated transversely (estimated as 3 times weaker from energy-resolved spatial PL). The difference in the coupling strength can be evidenced from the different visibility in the momentum-space interference fringes (implying synchronization) shown in the insets of Figs. 5(a) and 5(c).

Here, we investigate the polarization of the coupled condensates for each of the quasi-cw 50- μs excitation shots using a Wollaston prism and a detection camera. With the polarization resolving 100 shots, we observe distinct regimes depending on the separation distance between the condensates and their mutual orientation. For strongly coupled horizontally elongated traps separated by 26.5 μm , we observe approximately zero DOP in each shot [Fig. 5(d)] for each condensate (blue and red curves, respectively). On

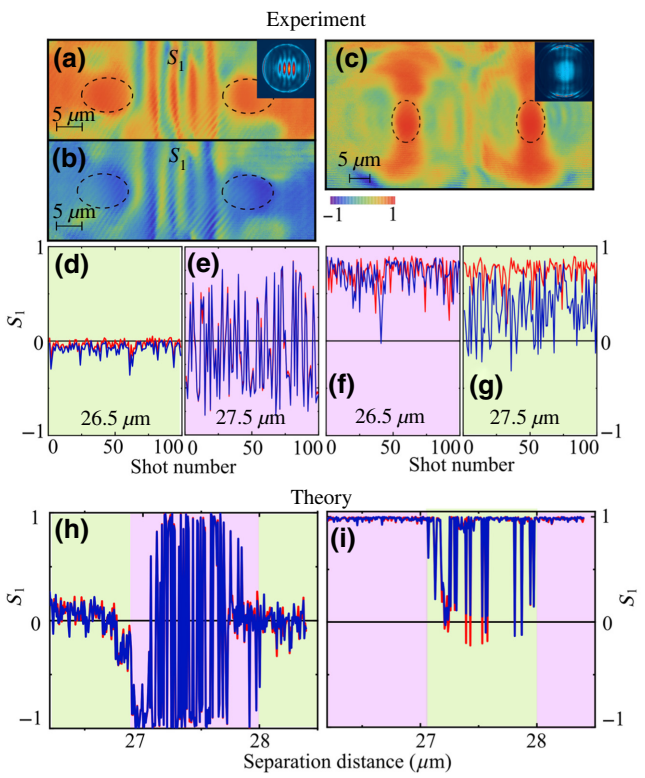


FIG. 5. The spatially resolved S_1 of coupled condensates oriented horizontally and separated by 27.5 μm for (a),(b) two different quasi-cw 50- μs excitation shots, showing the formation of either (a) horizontal or (b) vertical polarization in both condensates. (c) The spatially resolved S_1 from one realization of the two coupled condensates orientated vertically at 26.5 μm . The insets in (a) and (c) depict the corresponding k -space PL. (d),(e) One hundred time-integrated realizations (shots) of the S_1 for the left (blue) and right (red) condensate in the horizontal-horizontal major-axis configuration and (f),(g) in the vertical-vertical configuration. The experimental data are taken at approximately $1.8P_{\text{th}}$. The distance dependence of the S_1 from simulations corresponding to (h) horizontal-horizontal and (i) vertical-vertical major-axis configurations. Each data point represents one shot (time-averaged). The green and purple backgrounds in (d)–(i) illustrate regions of similar behavior between experiment and theory.

the other hand, at a 27.5- μm distance, we now observe a strong S_1 component stochastically flipping from shot to shot [Fig. 5(e)] with a small $S_{2,3}$ (for supplemental data on the other Stokes components, see Sec. S9 in the Supplemental Material [52]). In this case, both condensates adopt the same linear polarization, randomly changing between horizontal [Fig. 5(a)] and vertical [Fig. 5(b)] from shot to shot. Interestingly, the polarizations of the condensates are almost perfectly correlated (Pearson correlation coefficient $\rho = 0.99$), which implies that they are strongly coupled. Such random linear-polarization flipping suggests the presence of bistability in our system [7] triggered by the spatial coupling mechanism.

On the other hand, for the weakly coupled (vertically elongated) traps [see Fig. 5(c)], we observe qualitatively different behavior. If we choose the same distances again, we now see a strong positive S_1 component at 26.5 μm in each condensate [Fig. 5(f)], as one would expect for an isolated vertical trap. However, interestingly, at 27.5 μm we observe the appearance of semidepolarized behavior [Fig. 5(g)], evidenced through stronger polarization fluctuations from shot to shot. In both cases, due to the weaker spatial coupling, the condensates are no longer strongly correlated in their S_1 components, with $\rho = 0.5$ and $\rho = 0.26$ for the two studied distances, respectively. We point out the different average S_1 values between the left and the right condensates in Fig. 5(g), which we attribute to the position-dependent random birefringence $\Omega_{\text{bir}}(\mathbf{r})$.

B. Theory of coupled condensates

We reproduce our experimental observations through mean-field simulations on time-delayed coupled spinor polariton condensates. Here, we model the dynamics of each condensate spinor $\Psi = (\psi_+, \psi_-)^T$ using the generalized (driven-dissipative) Gross-Pitaevskii equation, coupled to a semiclassical rate equation describing a reservoir of low-momentum excitons $\mathbf{X} = (X_+, X_-)^T$ that scatter into the condensate [67]. The indexes (1) and (2) denote the left and right condensate, respectively:

$$\begin{aligned} i\frac{d\psi_{\pm}^{(1,2)}}{dt} &= \left[\omega_0 + \alpha|\psi_{\pm}^{(1,2)}|^2 + gX_{\pm}^{(1,2)} + i\frac{RX_{\pm}^{(1,2)} - \Gamma}{2} \right] \\ &\quad \times \psi_{\pm}^{(1,2)} + (\epsilon + i\gamma)\psi_{\mp}^{(1,2)} \\ &\quad + J\psi_{\pm}^{(2,1)}(t - \tau) + \mathcal{J}\psi_{\mp}^{(2,1)}(t - \tau), \\ \frac{dX_{\pm}^{(1,2)}}{dt} &= P - \left(\Gamma_R + R|\psi_{\pm}^{(1,2)}|^2 \right) X_{\pm}^{(1,2)} + \Gamma_s(X_{\mp}^{(1,2)} \\ &\quad - X_{\pm}^{(1,2)}). \end{aligned} \quad (5)$$

Here, α and g are the repulsive (defocusing) interaction constants describing the polariton-polariton and polariton-reservoir blue shift, R governs the stimulated scattering rate from the reservoir into the condensate, Γ and Γ_R are the polariton and exciton reservoir decay rates, Γ_s is the rate of spin relaxation within the reservoirs, ϵ and γ describe the complex-valued fine structure (taken here between horizontal and vertical polarized modes), and P denotes the nonresonant pumping power. For a linearly polarized cw pump, we can safely neglect the polarization and time dependence of any high-momentum exciton reservoirs describing excitons that are too energetic to scatter into the condensate [68]. We introduce the condensate intrinsic energy ω_0 , since a suitable rotating reference frame cannot be chosen for time-delayed coupled oscillators.

The intercondensate coupling, denoted by $J, \mathcal{J} \in \mathbb{C}$, is sometimes referred to as ballistic coupling and has recently been described through time-delayed coupled equations of motion [62]. Energetic polaritons escape from each trap and undergo finite-time free-space propagation before they reach their neighboring condensate. Such coupling becomes qualitatively different from evanescent coupling (e.g., tunneling between trapped Bose-Einstein condensates) when the propagation time τ of particles between condensates is comparable to their intrinsic frequencies. As has previously been demonstrated in Ref. [62], the strength of the coupling J depends on the separation distance d between the condensates,

$$J(d) = J_0|H_0^{(1)}(k_c d)|, \quad (6)$$

where $H_0^{(1)}$ is the zeroth-order Hankel function of the first kind, $J_0 \in \mathbb{C}$ quantifies the non-Hermitian coupling strength dictated by the overlap of the condensates over the optical trap region, and k_c is the complex wave vector of the polaritons propagating outside the optical trap:

$$k_c = k_c^{(0)} + i\frac{\Gamma m}{2\hbar k_c^{(0)}}. \quad (7)$$

From experiment, we estimate $k_c^{(0)} \approx 1.35 \mu\text{m}^{-1}$. This value corresponds to the radius of the outer momentum-space PL ring shown in Fig. 1(e). The imaginary term in Eq. (7) describes the additional attenuation of polaritons due to their finite lifetime and m is the polariton effective mass. We also account for coupling between the spins of the two condensates due to the TE-TM splitting, which is captured with the parameter \mathcal{J} . The time-delay parameter is approximated from the polariton phase velocity, which gives

$$\tau = \frac{2dm}{\hbar k_c^{(0)}}. \quad (8)$$

The results from simulations for both strongly and weakly coupled traps are presented in Figs. 5(h) and 5(i), respectively. We scan the distance d between the condensates (each data point is one shot using random initial conditions) and observe the periodic appearance of dramatically different dynamics (green and purple backgrounds) similar to the phase-flip transitions recently reported in Ref. [62].

For the strongly coupled traps, Fig. 5(h) indeed shows that—depending on distance—one can retrieve very low time-averaged polarization, which we will refer to as the unstable regime. There, a complex interplay of spin coupling and ballistic coupling results in the chaotic dynamics depicted in Fig. 6(a) and 6(b). Between 27 μm and 28 μm , a high-amplitude random S_1 component builds up from shot to shot due to the condensate spinors suddenly synchronizing, as depicted in Figs. 6(c) and 6(d). These results

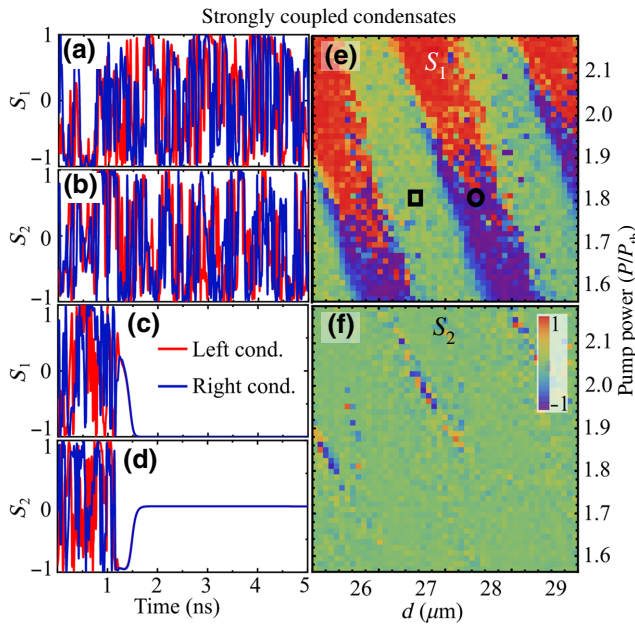


FIG. 6. The simulated time evolution of $S_1(t)$ and $S_2(t)$ for a single realization of the condensate at (a),(b) the black square and (c),(d) the black circle in Fig. 6(e), corresponding to the unstable and stable regimes, respectively. The red and blue colors correspond to the left and right condensates, respectively. (e),(f) Heat maps of the numerically obtained time-averaged Stokes parameters $S_{1,2}$ of one condensate from random initial conditions and varying pump power and distance.

are in qualitative agreement with those seen in experiment in Figs. 5(d) and 5(e). The parameters of the simulation are as follows: $\epsilon = -0.01 \text{ ps}^{-1}$; $\gamma = \epsilon/2$; $\Gamma = 0.25 \text{ ps}^{-1}$; $\Gamma_R = \Gamma/4$; $\Gamma_s = \Gamma_R/2$; $\alpha = 0.15\epsilon$; $R = 0.05\epsilon$; $\omega_0 = 5.5\Gamma$; $g = \alpha$; $m = 0.3 \text{ meV ps}^2 \mu\text{m}^{-2}$; $J_0 = 0.67e^{1.8i} \text{ ps}^{-1}$; and $\mathcal{J} = 0.2J$.

For the weakly coupled traps, we again obtain qualitative agreement between theory [Fig. 5(i)] and experiment [Figs. 5(f) and 5(g)]. As mentioned in Sec. IV A, the weak coupling between condensates is estimated to be 3 times smaller than the strong coupling. This is implemented in the simulation by simply scaling $J_0 \rightarrow J_0/3$. Now, strong $S_1 \approx 1$ regimes appear [purple background in Fig. 5(i)], interleaved with regimes of semidepolarized behavior [green background in Fig. 5(i)].

It is beyond the scope of the current study to provide an exhaustive analysis on the dynamics of the coupled condensates. We end this section by providing an insightful wider scan in distance and power in Figs. 6(e) and 6(f) for the case of strongly coupled condensates. Each pixel represents one realization of the time-averaged $S_{1,2}$ from the left condensate (the right condensate shows nearly identical behavior). The threshold power is derived for a single condensate as $P_{\text{th}} = (\Gamma - 2|\gamma|)\Gamma_R/R$. At high powers, we observe the condensates stabilizing into the ground state

(horizontal) polarization [red colors in Figs. 6(e) and 6(f)], whereas at low power we retrieve stable excited-state (vertical) polarization condensation [blue colors in Figs. 6(e) and 6(f)]. Between these regions, we observe an intermediate region (seen as a mixture of blue and red data points) where the ground- and excited-state condensates are both stable and the random initial condition determines the final state. This region corresponds to the experimental observation in Figs. 5(a), 5(b), and 5(e). We observe slanted regions of complete depolarization (green color) corresponding to the unstable regime. For completeness, supplemental numerical data are presented in Sec. S8 in the Supplemental Material [52].

V. CONCLUSIONS

We investigate the steady-state polarization dynamics of a polariton condensate in an elliptically shaped trapping potential created through optical nonresonant linearly polarized excitation. We demonstrate that the condensate polarization is determined by the lifted spin degeneracy of the trap levels due to the geometric ellipticity of the trap and TE-TM splitting. The condensate always forms with a linear polarization that follows the minor axis of the trap ellipse. By rotating the excitation profile, we rotate the condensate linear polarization around the equatorial plane of the Poincaré sphere. We then extend our system to a pair of coupled condensates, revealing rich physics of synchronization and desynchronization by tuning the condensate coupling strength through the trap anisotropy and/or spatial separation.

We believe that our results could provide one of the missing pieces of the puzzle for creating all-optical spin circuits in spinoptronic applications. Moreover, they pave the way toward coherent light sources with on-demand switchable linear polarization and studies on extended systems of interacting nonlinear optical elements with anisotropic coupling strength and adjustable fine structure. Here, the response of the SLM limits the polarization rotation speed. However, other approaches to modifying the laser profile with a much higher speed—for example, the interference of two Laguerre-Gaussian laser beams [69,70] with different wavelengths—could result in the generation of sources of coherent light with rotating polarization at gigahertz operation rates.

The data presented in this paper are openly available from the University of Southampton repository [71].

ACKNOWLEDGMENTS

We acknowledge the support of the United Kingdom Engineering and Physical Sciences Research Council (Grant No. EP/M025330/1 on Hybrid Polaritonics), the European Union Horizon 2020 program, through a FET

Open research and innovation action under Grant Agreement No. 899141 (PoLLoC), and by the Russian Foundation for Basic Research (RFBR) according to Research Project No. 20-02-00919. H.S. acknowledges the Icelandic Research Fund, Grant No. 217631-051.

-
- [1] A. Kavokin, J. J. Baumberg, G. Malpuech, and F. P. Laussy, *Microcavities* (OUP, Oxford, 2007).
- [2] J. Kasprzak, M. Richard, S. Kundermann, A. Baas, P. Jeambrun, J. M. J. Keeling, F. M. Marchetti, M. H. Szymańska, R. André, J. L. Staehli, V. Savona, P. B. Littlewood, B. Deveaud, and L. S. Dang, Bose-Einstein condensation of exciton polaritons, *Nature* **443**, 409 (2006).
- [3] I. A. Shelykh, A. V. Kavokin, Y. G. Rubo, T. C. H. Liew, and G. Malpuech, Polariton polarization-sensitive phenomena in planar semiconductor microcavities, *Semicond. Sci. Technol.* **25**, 013001 (2009).
- [4] T. Liew, I. Shelykh, and G. Malpuech, Polaritonic devices, *Phys. E: Low-Dimensional Syst. Nanostruct.* **43**, 1543 (2011).
- [5] L. Pickup, K. Kalinin, A. Askopoulos, Z. Hatzopoulos, P. Savvidis, N. Berloff, and P. Lagoudakis, Optical Bistability under Nonresonant Excitation in Spinor Polariton Condensates, *Phys. Rev. Lett.* **120**, 225301 (2018).
- [6] Y. del Valle-Inclan Redondo, H. Sigurdsson, H. Ohadi, I. A. Shelykh, Y. G. Rubo, Z. Hatzopoulos, P. G. Savvidis, and J. J. Baumberg, Observation of inversion, hysteresis, and collapse of spin in optically trapped polariton condensates, *Phys. Rev. B* **99**, 165311 (2019).
- [7] H. Sigurdsson, Hysteresis in linearly polarized nonresonantly driven exciton-polariton condensates, *Phys. Rev. Res.* **2**, 023323 (2020).
- [8] T. K. Paraïso, M. Wouters, Y. Léger, F. Morier-Genoud, and B. Deveaud-Plédran, Multistability of a coherent spin ensemble in a semiconductor microcavity, *Nat. Mater.* **9**, 655 (2010).
- [9] A. Amo, T. C. H. Liew, C. Adrados, R. Houdré, E. Giacobino, A. V. Kavokin, and A. Bramati, Exciton-polariton spin switches, *Nat. Photonics* **4**, 361 (2010).
- [10] R. Cerna, Y. Léger, T. K. Paraïso, M. Wouters, F. Morier-Genoud, M. T. Portella-Oberli, and B. Deveaud, Ultrafast tristable spin memory of a coherent polariton gas, *Nat. Commun.* **4**, 2008 (2013).
- [11] C. Leyder, M. Romanelli, J. P. Karr, E. Giacobino, T. C. H. Liew, M. M. Glazov, A. V. Kavokin, G. Malpuech, and A. Bramati, Observation of the optical spin Hall effect, *Nat. Phys.* **3**, 628 (2007).
- [12] R. Hivet, H. Flayac, D. D. Solnyshkov, D. Tanese, T. Boulier, D. Andreoli, E. Giacobino, J. Bloch, A. Bramati, G. Malpuech, and A. Amo, Half-solitons in a polariton quantum fluid behave like magnetic monopoles, *Nat. Phys.* **8**, 724 (2012).
- [13] M. Sich, L. E. Tapia-Rodriguez, H. Sigurdsson, P. M. Walker, E. Clarke, I. A. Shelykh, B. Royall, E. S. Sedov, A. V. Kavokin, D. V. Skryabin, M. S. Skolnick, and D. N. Krizhanovskii, Spin domains in one-dimensional conservative polariton solitons, *ACS Photonics* **5**, 5095 (2018).
- [14] K. G. Lagoudakis, T. Ostatnický, A. V. Kavokin, Y. G. Rubo, R. André, and B. Deveaud-Plédran, Observation of half-quantum vortices in an exciton-polariton condensate, *Science* **326**, 974 (2009).
- [15] S. Donati, L. Dominici, G. Dagvadorj, D. Ballarini, M. De Giorgi, A. Bramati, G. Gigli, Y. G. Rubo, M. H. Szymańska, and D. Sanvitto, Twist of generalized skyrmions and spin vortices in a polariton superfluid, *Proc. Natl. Acad. Sci.* **113**, 14926 (2016).
- [16] S. Dufferwiel, F. Li, E. Cancellieri, L. Giriunas, A. A. P. Trichet, D. M. Whittaker, P. M. Walker, F. Fras, E. Clarke, J. M. Smith, M. S. Skolnick, and D. N. Krizhanovskii, Spin Textures of Exciton-Polaritons in a Tunable Microcavity with Large TE-TM Splitting, *Phys. Rev. Lett.* **115**, 246401 (2015).
- [17] H. Ohadi, A. Dreismann, Y. Rubo, F. Pinsker, Y. del Valle-Inclan Redondo, S. Tsintzos, Z. Hatzopoulos, P. Savvidis, and J. Baumberg, Spontaneous spin bifurcations and ferromagnetic phase transitions in a spinor exciton-polariton condensate, *Phys. Rev. X* **5**, 031002 (2015).
- [18] O. Bleu, D. D. Solnyshkov, and G. Malpuech, Interacting quantum fluid in a polariton Chern insulator, *Phys. Rev. B* **93**, 085438 (2016).
- [19] H. Sigurdsson, Y. S. Krivosenko, I. V. Iorsh, I. A. Shelykh, and A. V. Nalitov, Spontaneous topological transitions in a honeycomb lattice of exciton-polariton condensates due to spin bifurcations, *Phys. Rev. B* **100**, 235444 (2019).
- [20] T. Gao, C. Antón, T. C. H. Liew, M. D. Martín, Z. Hatzopoulos, L. Viña, P. S. Eldridge, and P. G. Savvidis, Spin selective filtering of polariton condensate flow, *Appl. Phys. Lett.* **107**, 011106 (2015).
- [21] A. Dreismann, H. Ohadi, Y. del Valle-Inclan Redondo, R. Balili, Y. G. Rubo, S. I. Tsintzos, G. Deligeorgis, Z. Hatzopoulos, P. G. Savvidis, and J. J. Baumberg, A sub-femtojoule electrical spin-switch based on optically trapped polariton condensates, *Nat. Mater.* **15**, 1074 (2016).
- [22] A. Askopoulos, A. V. Nalitov, E. S. Sedov, L. Pickup, E. D. Cherotchenko, Z. Hatzopoulos, P. G. Savvidis, A. V. Kavokin, and P. G. Lagoudakis, All-optical quantum fluid spin beam splitter, *Phys. Rev. B* **97**, 235303 (2018).
- [23] E. S. Sedov, Y. G. Rubo, and A. V. Kavokin, Polariton polarization rectifier, *Light: Sci. Appl.* **8**, 1 (2019).
- [24] S. Mandal, R. Banerjee, E. A. Ostrovskaya, and T. C. H. Liew, Nonreciprocal Transport of Exciton Polaritons in a Non-Hermitian Chain, *Phys. Rev. Lett.* **125**, 123902 (2020).
- [25] J. M. Ostermann and R. Michalzik in *VCSELs: Fundamentals, Technology and Applications of Vertical-Cavity Surface-Emitting Lasers*, edited by R. Michalzik (Springer-Verlag, Berlin, 2013), p. 147.
- [26] M. Lindemann, G. Xu, T. Pusch, R. Michalzik, M. Hofmann, I. Žutić, and N. Gerhardt, Ultrafast spin-lasers, *Nature* **568**, 1 (2019).
- [27] M. Drong, T. Fördös, H. Jaffrès, J. Peřina, K. Postava, P. Ciompa, J. Pištora, and H.-J. Drouhin, Spin-VCSELs with Local Optical Anisotropies: Toward Terahertz Polarization Modulation, *Phys. Rev. Appl.* **15**, 014041 (2021).
- [28] J. Hu, L.-s. Li, W. Yang, L. Manna, L.-w. Wang, and A. P. Alivisatos, Linearly polarized emission from colloidal semiconductor quantum rods, *Science* **292**, 2060 (2001).

- [29] X. Wang, A. M. Jones, K. L. Seyler, V. Tran, Y. Jia, H. Zhao, H. Wang, L. Yang, X. Xu, and F. Xia, Highly anisotropic and robust excitons in monolayer black phosphorus, *Nat. Nanotechnol.* **10**, 517 (2015).
- [30] A. Lundskog, C.-W. Hsu, K. Fredrik Karlsson, S. Amloy, D. Nilsson, U. Forsberg, P. Olof Holtz, and E. Janzen, Direct generation of linearly polarized photon emission with designated orientations from site-controlled InGaN quantum dots, *Light: Sci. Appl.* **3**, e139 (2014).
- [31] D. N. Krizhanovskii, D. Sanvitto, I. A. Shelykh, M. M. Glazov, G. Malpuech, D. D. Solnyshkov, A. Kavokin, S. Ceccarelli, M. S. Skolnick, and J. S. Roberts, Rotation of the plane of polarization of light in a semiconductor microcavity, *Phys. Rev. B* **73**, 073303 (2006).
- [32] I. Gruzov, H. Sigurdsson, S. Baryshev, T. Ermakov, A. Askopoulos, and P. G. Lagoudakis, Optical orientation, polarization pinning, and depolarization dynamics in optically confined polariton condensates, *Phys. Rev. B* **102**, 125419 (2020).
- [33] H. Ohadi, E. Kammann, T. C. H. Liew, K. G. Lagoudakis, A. V. Kavokin, and P. G. Lagoudakis, Spontaneous Symmetry Breaking in a Polariton and Photon Laser, *Phys. Rev. Lett.* **109**, 016404 (2012).
- [34] J. J. Baumberg, A. V. Kavokin, S. Christopoulos, A. J. D. Grundy, R. Butté, G. Christmann, D. D. Solnyshkov, G. Malpuech, G. Baldassarri Höger von Högersthal, E. Feltin, J.-F. Carlin, and N. Grandjean, Spontaneous Polarization Buildup in a Room-Temperature Polariton Laser, *Phys. Rev. Lett.* **101**, 136409 (2008).
- [35] M. D. Martín, D. Ballarini, A. Amo, Ł. Kłopotowski, L. Viña, A. V. Kavokin, and R. André, Striking dynamics of II–VI microcavity polaritons after linearly polarized excitation, *Phys. Status Solidi (c)* **2**, 3880 (2005).
- [36] Ł. Kłopotowski, M. D. Martin, A. Amo, L. Vina, I. A. Shelykh, M. M. Glazov, G. Malpuech, A. V. Kavokin, and R. Andre, Optical anisotropy and pinning of the linear polarization of light in semiconductor microcavities, *Solid State Commun.* **139**, 511 (2006).
- [37] J. Kasprzak, R. André, L. S. Dang, I. A. Shelykh, A. V. Kavokin, Y. G. Rubo, K. V. Kavokin, and G. Malpuech, Build up and pinning of linear polarization in the Bose condensates of exciton polaritons, *Phys. Rev. B* **75**, 045326 (2007).
- [38] R. Balili, V. Hartwell, D. Snoke, L. Pfeiffer, and K. West, Bose-Einstein condensation of microcavity polaritons in a trap, *Science* **316**, 1007 (2007).
- [39] D. Read, T. C. H. Liew, Y. G. Rubo, and A. V. Kavokin, Stochastic polarization formation in exciton-polariton Bose-Einstein condensates, *Phys. Rev. B* **80**, 195309 (2009).
- [40] S. Gerhardt, M. Deppisch, S. Betzold, T. H. Harder, T. C. H. Liew, A. Predojević, S. Höfling, and C. Schneider, Polarization-dependent light-matter coupling and highly indistinguishable resonant fluorescence photons from quantum dot-micropillar cavities with elliptical cross section, *Phys. Rev. B* **100**, 115305 (2019).
- [41] M. Klaas, O. A. Egorov, T. C. H. Liew, A. Nalitov, V. Marković, H. Suchomel, T. H. Harder, S. Betzold, E. A. Ostrovskaya, A. Kavokin, S. Klembt, S. Höfling, and C. Schneider, Nonresonant spin selection methods and polarization control in exciton-polariton condensates, *Phys. Rev. B* **99**, 115303 (2019).
- [42] L. Xiang, X. Zhang, J. Zhang, Y. Huang, W. Hofmann, Y. Ning, and L. Wang, Vcsel mode and polarization control by an elliptic dielectric mode filter, *Appl. Opt.* **57**, 8467 (2018).
- [43] B. Gayral, J. M. Gérard, B. Legrand, E. Costard, and V. Thierry-Mieg, Optical study of GaAs/AlAs pillar microcavities with elliptical cross section, *Appl. Phys. Lett.* **72**, 1421 (1998).
- [44] K. D. Choquette and R. E. Leibenguth, Control of vertical-cavity laser polarization with anisotropic transverse cavity geometries, *IEEE Photonics Technol. Lett.* **6**, 40 (1994).
- [45] T. Pusch, E. La Tona, M. Lindemann, N. C. Gerhardt, M. R. Hofmann, and R. Michalzik, Monolithic vertical-cavity surface-emitting laser with thermally tunable birefringence, *Appl. Phys. Lett.* **110**, 151106 (2017).
- [46] J. Plumhof, T. Stöferle, L. Mai, U. Scherf, and R. Mahrt, Room-temperature Bose-Einstein condensation of cavity exciton-polaritons in a polymer, *Nat. Mater.* **13**, 247 (2013).
- [47] G. Panzarini, L. C. Andreani, A. Armitage, D. Baxter, M. S. Skolnick, V. N. Astratov, J. S. Roberts, A. V. Kavokin, M. R. Vladimirova, and M. A. Kaliteevski, Exciton-light coupling in single and coupled semiconductor microcavities: Polariton dispersion and polarization splitting, *Phys. Rev. B* **59**, 5082 (1999).
- [48] P. Cilibrizzi, A. Askopoulos, M. Silva, F. Bastiman, E. Clarke, J. M. Zajac, W. Langbein, and P. G. Lagoudakis, Polariton condensation in a strain-compensated planar microcavity with InGaAs quantum wells, *Appl. Phys. Lett.* **105**, 191118 (2014).
- [49] E. Wertz, L. Ferrier, D. D. Solnyshkov, R. Johne, D. Sanvitto, A. Lemaître, I. Sagnes, R. Grousson, A. V. Kavokin, P. Senellart, G. Malpuech, and J. Bloch, Spontaneous formation and optical manipulation of extended polariton condensates, *Nat. Phys.* **6**, 860 (2010).
- [50] G. Tosi, G. Christmann, N. G. Berloff, P. Tsotsis, T. Gao, Z. Hatzopoulos, P. G. Savvidis, and J. J. Baumberg, Sculpting oscillators with light within a nonlinear quantum fluid, *Nat. Phys.* **8**, 190 (2012).
- [51] A. Askopoulos, H. Ohadi, A. V. Kavokin, Z. Hatzopoulos, P. G. Savvidis, and P. G. Lagoudakis, Polariton condensation in an optically induced two-dimensional potential, *Phys. Rev. B* **88**, 041308 (2013).
- [52] See the Supplemental Material at <http://link.aps.org/supplemental/10.1103/PhysRevApplied.16.034014> for details on numerical simulations and additional experimental and numerical data. The Supplemental Material includes Refs. [53–56].
- [53] C. Antón, T. C. H. Liew, G. Tosi, M. D. Martín, T. Gao, Z. Hatzopoulos, P. S. Eldridge, P. G. Savvidis, and L. Viña, Energy relaxation of exciton-polariton condensates in quasi-one-dimensional microcavities, *Phys. Rev. B* **88**, 035313 (2013).
- [54] V. Flunkert, in *Delay-Coupled Complex Systems: and Applications to Lasers* (Springer-Verlag, Berlin, 2011) p. 153.

- [55] I. A. Shelykh, Y. G. Rubo, G. Malpuech, D. D. Solnyshkov, and A. Kavokin, Polarization and Propagation of Polariton Condensates, *Phys. Rev. Lett.* **97**, 066402 (2006).
- [56] E. Estrecho, T. Gao, N. Bobrovska, M. D. Fraser, M. Steger, L. Pfeiffer, K. West, T. C. H. Liew, M. Matuszewski, D. W. Snoke, A. G. Truscott, and E. A. Ostrovskaya, Single-shot condensation of exciton polaritons and the hole burning effect, *Nat. Commun.* **9**, 2944 (2018).
- [57] I. I. Ryzhov, V. O. Kozlov, N. S. Kuznetsov, I. Y. Chestnov, A. V. Kavokin, A. Tzimis, Z. Hatzopoulos, P. G. Savvidis, G. G. Kozlov, and V. S. Zapasskii, Spin noise signatures of the self-induced Larmor precession, *Phys. Rev. Res.* **2**, 022064 (2020).
- [58] C. Redlich, B. Lingnau, S. Holzinger, E. Schlottmann, S. Kreinberg, C. Schneider, M. Kamp, S. Höfling, J. Wolters, S. Reitzenstein, and K. Lüdge, Mode-switching induced super-thermal bunching in quantum-dot microlasers, *New J. Phys.* **18**, 063011 (2016).
- [59] M. Maragkou, C. E. Richards, T. Ostatnický, A. J. D. Grundy, J. Zajac, M. Hugues, W. Langbein, and P. G. Lagoudakis, Optical analogue of the spin Hall effect in a photonic cavity, *Opt. Lett.* **36**, 1095 (2011).
- [60] L. A. Smirnov, D. A. Smirnova, E. A. Ostrovskaya, and Y. S. Kivshar, Dynamics and stability of dark solitons in exciton-polariton condensates, *Phys. Rev. B* **89**, 235310 (2014).
- [61] M. Maragkou, A. J. D. Grundy, E. Wertz, A. Lemaître, I. Sagnes, P. Senellart, J. Bloch, and P. G. Lagoudakis, Spontaneous nonground state polariton condensation in pillar microcavities, *Phys. Rev. B* **81**, 081307 (2010).
- [62] J. Töpfer, H. Sigurdsson, L. Pickup, and P. Lagoudakis, Time-delay polaritonics, *Commun. Phys.* **3**, 2 (2020).
- [63] X. Qiao, B. Midya, Z. Gao, Z. Zhang, H. Zhao, T. Wu, J. Yim, R. Agarwal, N. M. Litchinitser, and L. Feng, Higher-dimensional supersymmetric microlaser arrays, *Science* **372**, 403 (2021).
- [64] H. Ohadi, A. Ramsay, H. Sigurdsson, Y. del Valle-Inclan Redondo, S. Tsintzos, Z. Hatzopoulos, T. Liew, I. Shelykh, Y. Rubo, P. Savvidis, and J. Baumberg, Spin Order and Phase Transitions in Chains of Polariton Condensates, *Phys. Rev. Lett.* **119**, 067401 (2017).
- [65] J. D. Töpfer, I. Chatzopoulos, H. Sigurdsson, T. Cookson, Y. G. Rubo, and P. G. Lagoudakis, Engineering spatial coherence in lattices of polariton condensates, *Optica* **8**, 106 (2021).
- [66] M. Pieczarka, E. Estrecho, S. Ghosh, M. Wurdack, M. Steger, D. W. Snoke, K. West, L. N. Pfeiffer, T. C. H. Liew, A. G. Truscott, and E. A. Ostrovskaya, Topological phase transition in an all-optical exciton-polariton lattice, *Optica* **8**, 1084 (2021).
- [67] M. Wouters and I. Carusotto, Excitations in a Nonequilibrium Bose-Einstein Condensate of Exciton Polaritons, *Phys. Rev. Lett.* **99**, 140402 (2007).
- [68] C. Antón, S. Morina, T. Gao, P. S. Eldridge, T. C. H. Liew, M. D. Martín, Z. Hatzopoulos, P. G. Savvidis, I. A. Shelykh, and L. Viña, Optical control of spin textures in quasi-one-dimensional polariton condensates, *Phys. Rev. B* **91**, 075305 (2015).
- [69] S. Franke-Arnold, J. Leach, M. J. Padgett, V. E. Lembessis, D. Ellinas, A. J. Wright, J. M. Girkin, P. Öhberg, and A. S. Arnold, Optical ferris wheel for ultracold atoms, *Opt. Express* **15**, 8619 (2007).
- [70] Y. V. Kartashov and D. A. Zezyulin, Rotating patterns in polariton condensates in ring-shaped potentials under a bichromatic pump, *Opt. Lett.* **44**, 4805 (2019).
- [71] I. Gnusov, H. Sigurdsson, J. D. Topfer, S. Baryshev, S. Alyatkin, and P. G. Lagoudakis, Data for: “All-optical linear-polarization engineering in single and coupled exciton-polariton condensates,” <https://doi.org/10.5258/SOTON/D1924> (2021).